found for the fit,

$$\hat{P} = -1.63 + 1.85m + 3.50d - 1.44tm - 0.0618ts + 3.99t^2 \quad (18)$$

Analysis of the contribution of the parameters t, d, m, and s has disclosed an ordering in their contribution to $\hat{P}$. The ordering is shown in Table 9. The purpose of this mathematical analysis was to discover the primary variables and their relative importance in relating to PIO. On the basis of the results, a complete simulation study is planned to gain further insight into the relationship between PIO and the characteristics of the step response.

References

[1] DiFranco, D. A., "In-Flight Investigation of the Effects of Higher-Order Control System Dynamics on Longitudinal Handling Qualities," AFFDL-TR 68-90, Aug. 1968, Cornell Aeronautical Lab., Buffalo, N.Y.

[2] McDonnel, A. A., "Pilot Rating Techniques for the Estimation and Evaluation of Handling Qualities," AFFDL-TR 68-76, Dec. 1968, Air Force Systems Command, Wright Patterson Air Force Base, Ohio.

JULY-AUG. 1970 J. AIRCRAFT VOL. 7, NO. 4

Flutter Induced by Aerodynamic Interference Between Wing and Tail

O. SENSBURG*
Messerschmitt Bölkow Blohm GmbH, München, Germany

AND

B. LASCHKA†
Vereinigte Flugtechnische Werke-Fokker GmbH, München, Germany

Several authors have mentioned that aerodynamic interference between horizontal tail and wing could cause flutter. The unsteady aerodynamic forces pose the problem in analysis and have become available only recently. Naturally, the importance of interaction between two lifting-surface increases when both spans are of comparable magnitude. Several advanced aircraft feature this concept. A flutter analysis based on a variable-geometry airplane at highly swept condition is performed. The unsteady loads resulting from aerodynamic interference are introduced. They were determined with a lifting-surface method previously formulated by the coauthor. Destructive flutter was discovered resulting entirely from interference not predictable by applying conventional three-dimensional coefficients for the separate surfaces only. This verified a flutter case of a preceding experiment. The investigation is extended to include different vertical and aft positions of the horizontal tail at several Mach numbers to obtain an understanding of dominating influences.

Introduction

TWO years ago, Topp et al.[9] referred to an antisymmetric flutter case as experienced in a wind-tunnel test of an aircraft with variable wing geometry; see Fig. 1. This condition could not be determined theoretically by using conventional flutter approaches. After careful consideration of all prevailing influences, the instability was assumed to be due to the aerodynamic interference of wing and tail. No proof was given for this assumption, since at that time no method for the calculation of unsteady interference air loads was available, though H. Ashley had stimulated investigations in this field by a basic paper[1] as early as 1964.

In the meantime, B. Laschka and H. Schmid[6,10] investigated the aerodynamic interaction between oscillating wings and tails applying lifting-surface kernel function methods. It has been shown there that interference can be of considerable influence not only in the case of close proximity but also for large distances between wing and tail. Another approach by V. J. E. Stark[2] is based on lifting line lattices. Application has been reported by H. Wittmeyer[11] for the SAAB 37 Viggen flutter analysis. A similar procedure has also been proposed by E. Albano and W. Rodden.[3]

The amplitudes of the wing oscillation are usually small in the region near the body and high near the wing tip. Thus, high induced-velocity components usually can be expected downstream from the wing tip. Consequently, interference in most cases will become important where the span of the tail is not small relative to the wing span. Configurations showing these features are found on many modern airplanes especially on those with variable-geometry wings, or canard types. Conventional flutter analysis took into account the natural modes, generalized masses, and stiffnesses of the entire aircraft and applied the nonsteady airloads to wing and tail without interference effects. In the present paper, these interference effects no longer are neglected.

Flutter behavior on the variable geometry (VG) airplane configuration mentioned in Ref. 9 has been studied for the most critical case where the wing had a leading edge (LE) sweep of 70°. Theoretical analysis indicates a destructive flutter case resulting entirely from aerodynamic interaction that could not be predicted by applying only conventional three-dimensional aerodynamic coefficients to wing and horizontal tail separately. The experimentally experienced flutter case[9] thus could be verified. This result is of considerable interest, since before this investigation the question was raised as to

Presented at the AIAA Structural Dynamics and Aeroelasticity Specialist Conference, New Orleans, La., April 17–19, 1969; submitted May 13, 1969; revision received October 29, 1969.

* Chief Engineer, Flutter Department.

† Head, Technical Research Department.

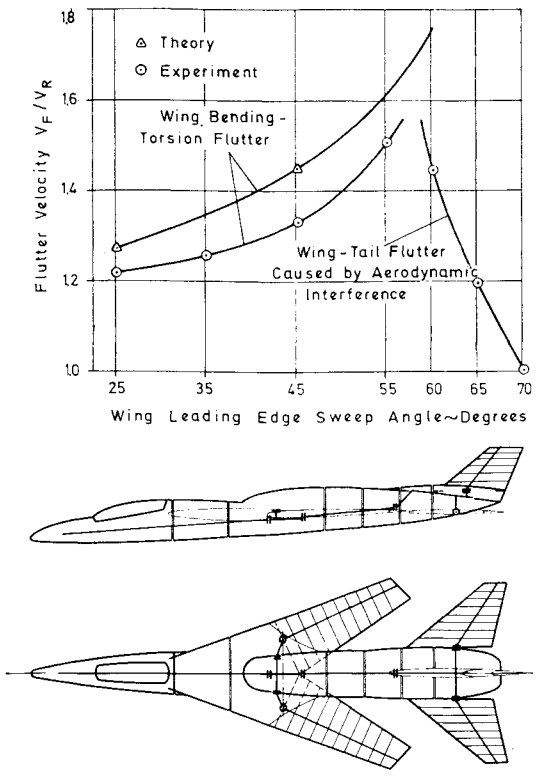

Fig. 1 Flutter velocity V_F/V_R vs wing sweep as given in Ref. 9 for a variable geometry aircraft (V_R = flutter speed for 70° sweep).

whether flutter was caused by the interference actually based on potential flow or rather by the high energy leading edge vortices that are connected with highly swept wings and that cannot be predicted by linearized theory.

In addition, the influence of the vertical and streamwise position of the tail was studied. The general opinion that increased aft position of the horizontal stabilizer increases flutter speed could not be substantiated. On the contrary, the calculated results show a decrease in critical speed with increasing aft position of the tail for the present configuration. Finally, the calculated damping characteristics showed that by including aerodynamic interference a moderate flutter case was changed into an explosive one. This corresponds to observations made during wind-tunnel tests.

Analysis

Flutter Equation

The analysis is based on the conventional flutter equation

$$[M - (1/\omega^2 + ig/\omega^2)K + A]q = 0 \qquad (1)$$

where M stands for the matrix of generalized masses, K is the matrix of generalized stiffnesses. A is the matrix of generalized aerodynamic forces, q is a generalized coordinate, ω is the circular frequency, and $i = (-1)^{1/2}$ the imaginary unit. Air loads resulting from harmonic oscillations are introduced as unsteady air load matrix A. The matrix igK/ω^2 introduced into the oscillating system representing the aircraft has to be interpreted as the generalized damping force necessary to maintain harmonic oscillation.

Vibration Analysis

The natural vibration modes, generalized stiffnesses, and masses were determined by calculation and by means of a ground vibration test. The model was constructed from movable panels and beams carrying discretely attached additional masses; see Fig. 1. The vibration analysis therefore could make use of the conventional beam theory.

Table 1 Calculated and measured frequencies and generalized masses

	Frequency, cps		Generalized mass	
No.	Calculated	Measured	Calculated	Measured
1	6.26	5.62	5.52	4.47
2	6.93	6.24	4.02	6.20
3	8.60	8.25	2.14	2.93
4	9.73	9.22	0.33	0.445
5	16.46	14.60	2.92	0.855
6	18.65		0.89	
7	18.81		1.11	
8	20.14		0.18	
9	20.81		0.72	
10	23.67		1.45	

By using 27 individual degrees of freedom of the five components, i.e., forward fuselage section, wing, horizontal tail, and vertical tail, the first ten antisymmetrical vibration modes were determined theoretically. Comparison with the natural vibration modes measured during the ground vibration test showed good correlation for the first four modes (see Table 1). For higher modes differences occurred that could be traced to simplifying assumptions in the theory as well as to inaccuracies in the model and the limited number of shakers used in the vibration test.

Unsteady Aerodynamic Forces

The generalized aerodynamic forces of mutually interferring lifting surfaces can be described by a matrix diagram with the usual assumptions of linearized potential flow. Oscillations of a surface in an air flow not only cause pressures on the surface itself but also induce a flowfield in its vicinity. If a second surface is located in this field, then it will experience induced pressures. The resulting pressure is obtained by linear superposition of the pressure induced by a surface itself and pressures induced by separate surfaces. For a system represented by wing (A), horizontal tail (B), and vertical tail (C), Table 2 applies.‡

In Refs. 10 and 6, calculation methods for these generalized forces were developed, based on the lifting-surface theory (Ref. 4), and are explained here in their basic concept. The velocity field (u, v, w) induced by lifting surface (F) located approximately in the plane $z = 0$ may be described by, e.g., Ref. 5:

$$\begin{Bmatrix} u(x,y,z) \\ v(x,y,z) \\ w(x,y,z) \end{Bmatrix} = \frac{1}{8\pi} \exp(ikt) \iint_{(F)} \Delta c_p(x',y') \times \begin{Bmatrix} E(x_0,y_0,z;\ M,k) \\ H(x_0,y_0,z;\ M,k) \\ K(x_0,y_0,z;\ M,k) \end{Bmatrix} dx'dy' \qquad (2)$$

An explanation of the terms may be found in Fig. 2; Δc_p is the pressure difference between the upper and lower side of the surface, k is the reduced frequency, t is dimensionless time, M is the Mach number. Here the induced velocities are referred to the flow velocity V far upstream of the wing, and all lengths are referred to the semispan of the wing. E, H, and K are influence functions of the downwash, sidewash, and streamwise velocity component defined in Ref. 5. They are obtained by applying the differential operator $\nabla = [(\partial/\partial x), (\partial/\partial y), (\partial/\partial z)]$ to the influence functions D of the potential

$$(E;\ H;\ K) = \nabla D \qquad (3)$$

‡ The first index relates to the surface on which the aerodynamic forces occur; the second index relates to the surface that induces these forces. The same applies to the velocities defined below in Eqs. (13).

Table 2 Generalized forces acting on wing, horizontal tail, and vertical tail

Generalized forces		Induced by mode of: Wing	Horizontal tail	Vertical tail
Induced on	Wing	A_{AA}	A_{AB}	A_{AC}
	Horizontal tail	A_{BA}	A_{BB}	A_{CB}
	Vertical tail	A_{CA}	A_{CB}	A_{CC}

$$D(x_0,y_0,z;\ M,K) = \exp(-ikx_0)(kz/r)\Big\{K_1(kr) + (\pi i/2) \times [I_1(kr) - L_1(kr) - (2/\pi)] + (x_0/krR) \times \exp[(ik/\beta^2)(x_0 - MR)] - i\int_0^{(x_0-MR)/\beta^2 r} \times (1+\tau^2)^{-1/2}\cdot\tau\exp(ikr\tau)d\tau\Big\} \quad (4)$$

where $x_0 = x - x'$, $y_0 = y - y'$ and $r^2 = y_0^2 + z^2$, $R^2 = x_0^2 + \beta^2 r^2$, $\beta^2 = 1 - M^2$, and I_1, K_1 are modified Bessel functions of the first and second kind and the Struve function L_1. For $z = 0$, the sidewash and the streamwise velocity components result:

$$u(x,y,0) = [\exp(ikt)/4](z/|z|)\Big[\Delta c_p(x,y) - ik\int_{x_{LE}(y)}^{x}\Delta c_p(x',y)\exp(-ikx_0)dx'\Big] \quad (5)$$

$$v(x,y,0) = [\exp(ikt)/4](z/|z|)(\partial/\partial y)\int_{x_{LE}(y)}^{x} \times \Delta c_p(x',y)\exp(-ikx_0)dx' \quad (6)$$

whereas for the upwash Eq. (2) remains valid if there the limit $z \to 0$ is performed in the kernel function $K(x_0, y_0, z;\ k)$.

This kernel function is identical with the known form given by Watkins et al.[7] and it appears in the lifting-surface equation used to determine the pressure for a given upwash. The upwash acting on the wing results from the boundary condition derived from the vibration mode $z_F(x,y)$:

$$w(x,y,0) = (\partial z_F/\partial x) + ikz_F \quad (7)$$

If the pressure distribution is known, it is possible to determine the induced velocity components by integration in accordance with Eq. (2). In Ref. 10 and Ref. 6, the following series were selected for the pressure distribution:

$$\Delta c_p(x,y) = \sum_{r=0}^{R}[4a_r(y)/l(y)]h_r(X) \quad (8)$$

$$h_r(X) = (2/\pi)[\cos r\varphi + \cos(r+1)\varphi]/\sin\varphi$$
$$X = [x - x_{le}(y)]/l(y) = (1/2)(1 - \cos\varphi) \quad (9)$$

$$a_r(y) = \sum_{\mu=1}^{m} A_{\mu r}\sin\mu$$

$$A_{\mu r} = (2/m+1)\sum_{n=1}^{m} a_r(\varphi_n)\sin\mu$$
$$y = \cos\vartheta;\ \vartheta_n = [n\pi/(m+1)] \quad (10)$$

Calculation of the velocities may thus be reduced to simple summation formulas.

$$\begin{Bmatrix}u(x,y,z)\\v(x,y,z)\\w(x,y,z)\end{Bmatrix} = \sum_{r=0}^{R}\sum_{n=1}^{m} a_r(y_n) \times \begin{Bmatrix}f_{ur}(x,y,z;\ y_n i k,M)\ q_u(y,z;\ y_n)\\f_{vr}(x,y,z;\ y_n i k,M)\ q_v(y,z;\ y_n)\\f_{wr}(x,y,z;\ y_n i k,M)\ q_w(y,z;\ y_n)\end{Bmatrix} \quad (11)$$

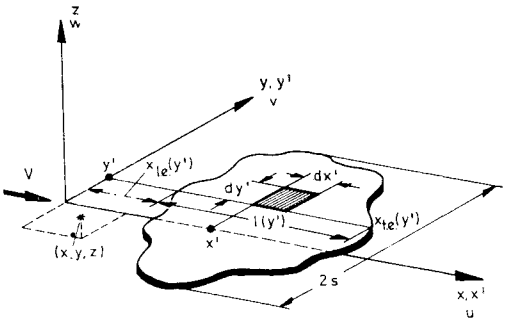

Fig. 2 Coordinate system introduced.

In this case, q_u, q_v, and q_w represent integration constants that vary only with y and z, while the dependence of x, k, M, and the rth term of the pressure distribution series is separated into the functions f_{ur}, f_{vr}, and f_{wr}.§

A considerable reduction in calculation effort is possible if the flowfield is required at medium or large distances from the wing and not in close proximity. The kernel functions then are surprisingly simple. These "asymptotic kernel functions" E, H, and K are obtained by considering Eq. (3), if the following equation is used for the influence function D of the potential instead of Eq. (4)¶ (see Ref. 5).

$$D(x_0,y_0,z;\ k) \approx [1 + (x/|x|)]k^2\exp(-ikx_0)(z/kr)K_1(kr)$$
$$\text{for } (x - x_{TE}) > l(y);\quad (x - x_{LE}) < l(y) \quad (12)$$

For $z = 0$, Eqs. (5) and (6) remain valid. These kernel functions show that the velocity components upstream of the wing disappear rapidly; downstream of the wing, however, they oscillate harmonically as a function of x. Furthermore, with the asymptotic kernel function a Mach number effect no longer appears in the velocity components. A Mach number effect shows up only in the pressure distribution.

A surprising outcome of the investigations performed in Ref. 10 was the fact that already at distances of approximately one wing chord downstream of the trailing edge (TE), the "asymptotic kernel functions" provide almost the exact velocities. This is of great importance for application in actual design, since most recent aircraft configurations have wing-tail distances satisfying this condition. This result is shown for low and high Mach numbers in Fig. 3. The real and imaginary part of the downwash obtained with the asymptotic influence function and exact influence functions for $M = 0$ and $M = 0.9$ is plotted vs the streamwise coordinate for several spanwise stations. For $M = 0.9$, the same pressure distribution was assumed as for $M = 0$ so that the compressibility effect that rapidly disappears with increasing downstream distance is made apparent.

The upwash obviously can reach large values. If there is a second surface located in this wake it must experience con-

§ Integration over x' can be performed with the Gauss-Jakobi quadrature. The integrand is subject to drastic changes in spanwise direction. This is attributable to the terms of the order $(z^2/r^4, zy_0/r^4, 1/r^2, \ln r)$ occurring in the kernel function. These can be separated and treated individually.

¶ $E(x_0,y_0,z;\ k) \approx -[1 + (x/|x|)]k^2\exp(-ikx_0) \times (iz/r)K_1(kr)$

$H(x_0,y_0,z;\ k) \approx -[1 + (x/|x|)]k^2\exp(-ikx_0)zy_0/r_2\,[K_0(kr) + (2/kr)K_1(kr)]$

$K(x_0,y_0,z;\ k) \approx -[1 + (x/|x|)]k^2\exp(-ikx_0) \times \{(z^2/r^2)K_0(kr) - [(y_0^2 - z^2)/(kr^3)]K_1(kr)\}$

With this kernel function and with the pressure series in Eqs. (8–10), it is possible to perform exact chordwise integration. The result leads to Bessel functions of the zeroth and first order.

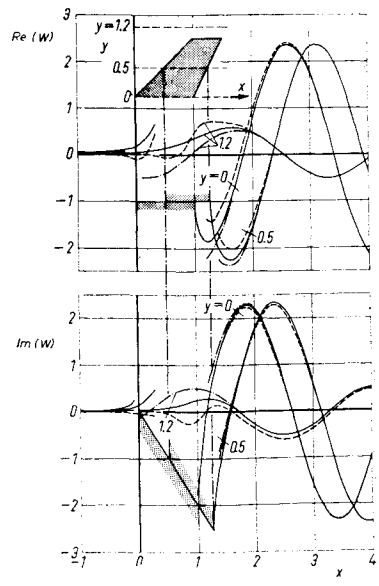

Fig. 3 Unsteady upwash distribution vs x axis on a swept wing (aspect ratio 2.667, taper ratio 0.5, leading edge sweep 45°) oscillating in pitch ($z = xe^{ikt}$): Exact kernel function — $M = 0$; ---- $M = 0.9$; Asymptotic kernel function - .- .- .- $0 \leqq M < 1$.

siderable induced pressures. Owing to the upwash, which varies considerably with x, the aft position of the tail unit is of importance for the magnitude and phase of the wing-induced pressure. Up to present it was accepted that the induced upwash attenuates rapidly as vertical distance increases. Although amplitudes decrease, noticeable influences remain present even at vertical distances on the order of one-half to one semispan, as may be seen from Table 3.

The mutual interference of several surfaces can be represented by adding the upwash portion induced by the other surfaces to the self-induced upwash component. If the surfaces are not all located in parallel planes, then all three components contribute to the normal velocities. A coupled integral equation system then results in accordance with the number of surfaces. For a horizontal tail (B) being parallel to wing (A) and for a vertical tail (C) lying in their plane of symmetry, one obtains the integral equation system for Δc_{pA}, Δc_{pB}, and Δc_{pC}.

$$\text{Wing:} \quad (\partial z_A/\partial x) + ikz_A = w_{AA}(\Delta c_{PA}) + w_{AB}(\Delta c_{PB}) + v_{AC}(\Delta c_{PC}) \quad (13a)$$

$$\text{Horizontal tail:} \quad (\partial z_B/\partial x) + ikz_B = w_{BA}(\Delta C_{PA}) + w_{BB}(\Delta c_{PB}) + v_{BC}(\Delta c_{PC}) \quad (13b)$$

$$\text{Vertical tail:} \quad (\partial z_C/\partial x) + ikz_C = v_{CA}(\Delta c_{PA}) + v_{CB}(\Delta c_{PB}) + w_{CC}(\Delta c_{PC}) \quad (13c)$$

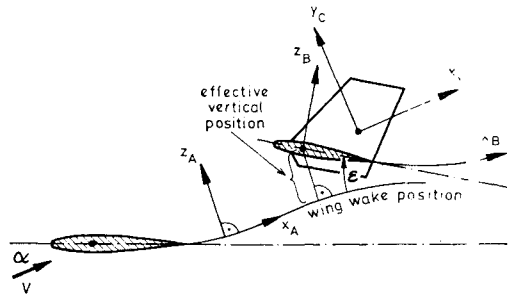

Fig. 4 Sketch of the coordinate systems of combined wing-tail system.

Table 3 Wing-induced rolling moments L_{BA} on the horizontal tail for different vertical positions based on asymptotic kernel function (basic horizontal position)

z/s_A	L_{BA}
0	−0.518 − i0.231
0.086	−0.383 − i0.170
0.255	−0.219 − i0.098

Indices were given previously in the footnote marked.‡ Since the vertical tail is normal to the other two surfaces, the induced normal component is formed by its self-induced portion of the upwash w_{CC} and the sidewash portion v_{CA} of the wing and v_{CB} of the horizontal tail. This applies, accordingly, to the effect of the vertical tail on wing and horizontal tail (v_{AC}, v_{BC}). The individual velocity components w_{AA}, w_{AB}, w_{AC}, w_{BA} . . . can be expressed for wing, vertical tail, and horizontal tail by means of the integral relations (2) or the summation formulas (11) and then introduced into Eqs. (13). When determining v_{AC}, v_{BC}, and w_{CC}, one should note that the direction of the y axis of the vertical tail is identified with that of the z axis of wing and horizontal tail and vice versa. Thereby, the linear system of equations can be solved for the unknown aerodynamic coefficient $(a_{rn})_A$, $(a_{rn})_B$, and $(a_{rn})_C$. This may be done either directly or by an iterative procedure. For wing and vertical tail symmetrical to the plane $y = 0$, no effect on and from the vertical tail will occur during symmetrical vibration modes of wing and horizontal tail. Thus, the third equation in Eqs. (13) and the components v_{AC} and v_{BC} will be eliminated. See Refs. 10 and 6 for the solution of the integral equation system.

When trying to find the generalized forces according to Table 1, A_{AA}, A_{BA}, and A_{CA} will be obtained by determining the pressure distributions for the vibration mode z_A of the wing according to Eqs. (13), for which distribution the vibration modes of the vertical and horizontal tail $z_B = z_C = 0$. This applies accordingly to A_{AB}, A_{BB}, A_{CB} and A_{CA}, A_{CB}, A_{CC}. When using asymptotic kernel functions, we get $A_{AB} = A_{AC} = 0$.

Some refinements of the present procedures have been investigated; see Fig. 4. Generally, the horizontal tail is inclined at an angle ϵ toward the wing. Consequently, the streamwise velocity component induced by the wing contributes to the normal component of the aerodynamic force of the horizontal tail, i.e., $u_{BA} \sin\epsilon$. Since the streamwise velocity component does not decrease in unsteady flow with increasing distance from the wing, which is contrary to its behavior in steady flow [see Eq. (5)], and it can, as a matter of fact, reach the magnitude of the upwash, it gains some importance for higher values of ϵ. A similar situation exists for the vertical tail provided there is an inclination out of the plane of symmetry of wing and tail unit.

The effect of the steady pitch angle also may be considered to some extent. The coordinate system (x_C, y_C, z_C) at the vertical tail has to be selected for the determination of the velocity components according to Eq. (11) such that the x_C axis coincides with the direction of the inflow velocity. A change of the pitch angle will result in a sweep angle change.

The wake may induce a still greater effect. Considerations have so far been based upon the purely linear theory, where the wake coincides with the mean plane of the lifting surface. The actual wake deforms in the direction of free inflow and, as is known, tends to roll up. The distortion (without lateral rolling up) depends upon the spanwise station, and at positive angles of attack will cause a greater interference effect in the case of a tail unit with elevated vertical position. This effect can approximately be taken into account by assuming the actual position of the tail unit relative to the steady wake position to be the effective vertical position to which the unsteady wake will be superimposed. A method and computer program exist for calculating the deformation of

Table 4 Rolling moments L_{AA}, L_{AB}, L_{BA}, and L_{BB} for coplanar wing and horizontal tail (basic horizontal position)

	L_{AA}	L_{AB}
Exact kernel function	$-0.406 + i0.918$	$-0.00006 + i0.009$
Asymptotic kernel function	$-0.393 + i0.920$	— —
	L_{BA}	L_{BB}
Exact kernel function	$-0.514 - i0.236$	$-0.144 + i0.632$
Asymptotic kernel function	$-0.518 - i0.231$	$-0.130 + i0.634$

the steady vortex layer by taking into account the mutual interference of wing and tail unit[8]. They have been repeatedly applied to current projects.

Scope of Analysis and Input Data

The configuration examined corresponds to the wind-tunnel model at maximum wing sweep (Fig. 1). In the investigation the influence of the following parameters on flutter velocity was analyzed: 1) variation of the vertical position of the horizontal tail (see Fig. 5); 2) variation of the aft position of the horizontal tail (see Fig. 5); 3) variation of Mach number $M = 0.25; 0.8; 0.95$; 4) vibration modes obtained from vibration analysis and ground vibration test; 5) variation of rigid body roll frequency. A flutter calculation was performed with the first ten antisymmetrical natural vibration modes, the rigid body roll mode being added as another degree of freedom. The corresponding aerodynamic forces were determined by the method described briefly in the preceding section for the idealized configuration without fuselage as shown in Fig. 5. Wing and horizontal tail were extended to the fuselage centerline; however, when integrating the pressure distribution in order to determine the generalized aerodynamic forces on the horizontal tail the section covered by the fuselage was left out. At first the vertical tail influence both on flutter velocity and on the damping characteristics of the basic configuration was taken into account by introduction of the self-induced forces A_{CC}. As the results thus obtained did not differ essentially, these forces were omitted in subsequent variations. Thus, it was required only to determine the aerodynamic force matrices A_{AA}, A_{AB}, A_{BA}, A_{BB}. The exact kernel function was used to calculate the aerodynamic forces for the different aft positions whereas, for the different vertical positions, the asymptotic kernel function was used offering excellent accuracy and considerably reducing computer time and costs.

Results

The order of magnitude of the occuring generalized aerodynamic forces can be seen from Tables 3 and 4. The numerical values for rigid body roll oscillation are compiled according to Table 2 for the rolling moment of wing and horizontal tail of the basic configuration. All values are related to the wing rolling moment without interference, where the reduced frequency $k = \omega \cdot s_A/V = 1.03$ and Mach number $M = 0.25$ apply. From Tables 3 and 4, it can be seen that the aerodynamic interference forces on the tail unit reach the magnitude of the self-induced aerodynamic forces. As compared to the asymptotic kernel function, use of the exact kernel function (Table 4) does not result in increased accuracy even with this close aft position.

The most important results of the present analysis are to be seen from Fig. 6, where, for the basic configuration, damping is shown vs freestream velocity. The aerodynamic forces have been calculated for $M = 0.25$ at sea level. Without aerodynamic interference, damping increases considerably, thereby eliminating any potential flutter. In case of interference, however, damping will begin to decrease at a certain

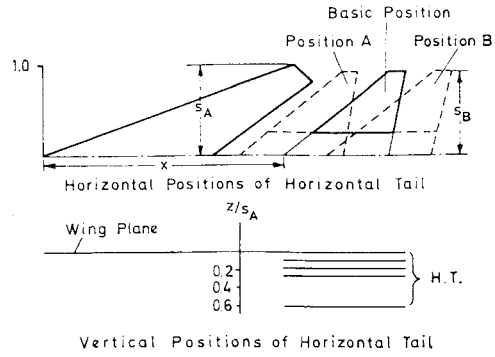

Fig. 5 Sketch of the investigated positions of the horizontal tail.

velocity; this decrease is the greater the smaller the vertical distance of the tail unit is relative to the wing. Flutter occurs in the case of a coplanar arrangement. This result is achieved by means of the input data obtained from the vibration analysis and also with those from the ground vibration test. With the latter data, a reduction of the critical velocity by approximately 5% results. In this case, it seems to be of interest, however, that the damping coefficient reaches higher values within the unstable range and reaches its maximum far less rapidly than with data obtained from the vibration analysis.

The flutter speed obtained from tests confirms the analysis. The value is somewhat higher than is to be expected from theory. Besides idealization inherent in theory, another reason might be given by the fact that the onset of flutter could not be defined clearly in the experiment performed. Undamped vibrations occurred already at somewhat lower speeds than those leading to destruction. The structural damping of the model results in a further, though small, increase in flutter speed.

The results described above were obtained without considering the aerodynamic forces of the vertical tail, which are expected to contribute to damping. Introducing them into subsequent calculation, however, resulted in a negligible change of the damping pattern; see Fig. 6. Without consideration of interference, a modification of Mach number (see Fig. 7) for values obtained from the vibration analysis shows the expected increase in damping. When considering

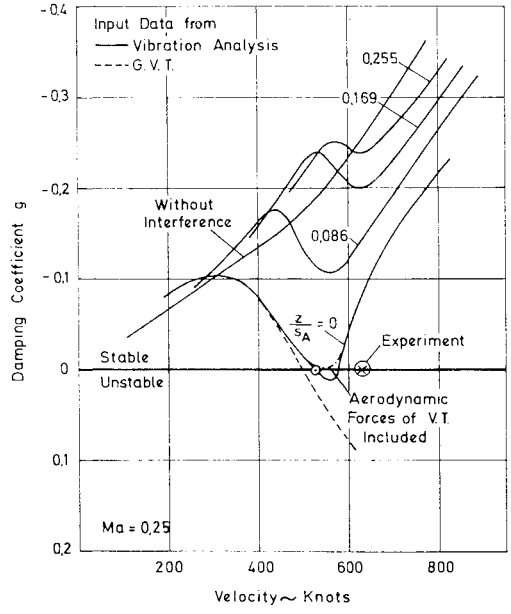

Fig. 6 Damping coefficient vs velocity for different vertical positions of the horizontal tail.

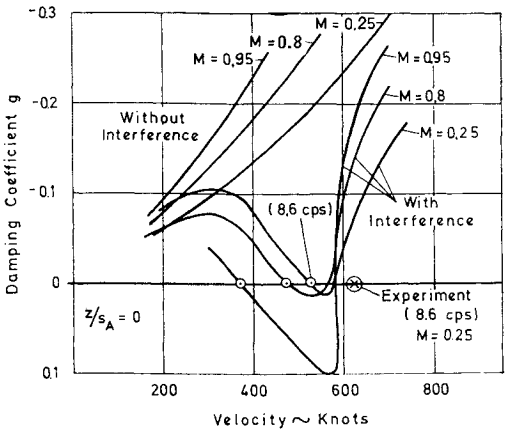

Fig. 7 Damping coefficient vs velocity for different Mach numbers.

interference, results are somewhat contradictory to those mentioned above. They indicate that the Mach number effect considerably reduces flutter speed of the aircraft under consideration.

It would seem logical to assume that an increased aft position of the tail unit will result in higher flutter speeds. The upwash distributions in Fig. 3 indicate that this is not always the case. Actually, the analysis of the case under consideration proves just the opposite; see Fig. 8. Flutter speed decreases with increasing distance between wing and tail unit. No flutter occurs at position A. For this analysis, the stiffness and mass matrices remained unchanged for all aft positions; thus, the plots represent merely the aerodynamic effects. Because of the nearly periodic upwash pattern in flow direction, the tendency shown in Fig. 8 will reverse for still larger aft positions. It is noteworthy that the flutter range shown in Fig. 8 will shift towards smaller aft positions and be considerably broadened because of the results from Fig. 6, when this analysis is conducted with the results from

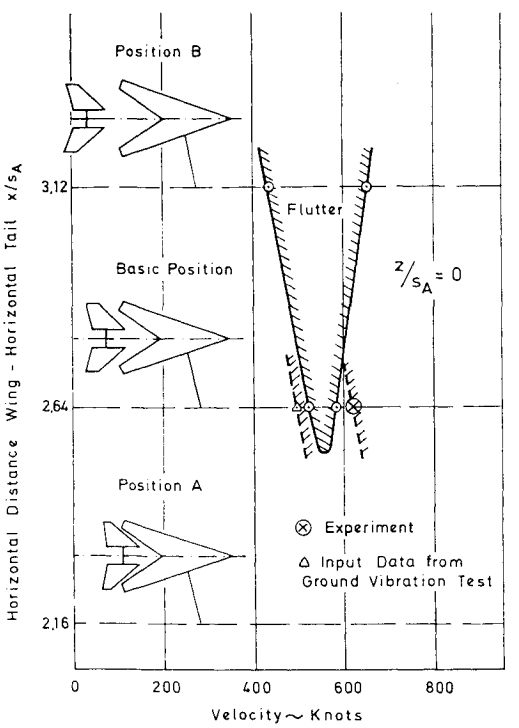

Fig. 8 Flutter speed vs horizontal distance between wing and horizontal tail.

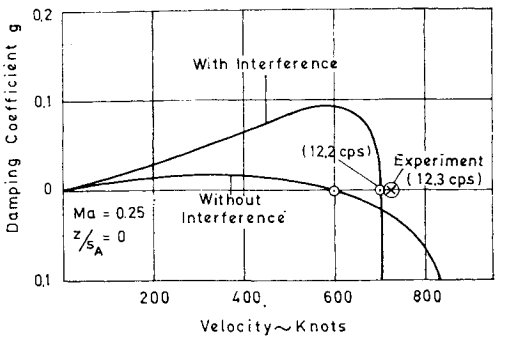

Fig. 9 Damping coefficient vs velocity for the horizontal tail flutter mode.

the ground vibration tests instead of the present theoretical values.

Finally, Fig. 9 shows the damping patterns of a horizontal tail unit flutter mode with only a small contribution of the wing. This pattern resulted from modifying the stiffness values of the horizontal tail. Damping gradients in the proximity of the flutter point are of some importance for flight flutter test. The inclusion of interference effects shows a sudden drop in damping in contrast with the smooth curve obtained without interference. This behavior pattern was visually observed during the corresponding wind-tunnel test.

References

[1] Ashley, H., "Some recent developments in interference theory for aeronautical applications," *Archiwum Mechaniki Stosowanej*, Vol. 16, 1964, pp. 149–178.

[2] Landahl, M. T. and Stark, V. J. E., "Numerical lifting surface theory—problems and progress," *AIAA Journal*, Vol. 6, No. 11, Nov. 1968, pp. 2049–2060.

[3] Albano, E. and Rodden, W., "A doublet lattice method for calculating lift distributions on oscillating surfaces in subsonic flow," *AIAA Journal*, Vol. 7, No. 2, Feb. 1969, pp. 279–285.

[4] Laschka, B., "Zur Theorie der harmonisch schwingenden tragenden Fläche bei Unterschallströmung," *Zeitschrift für Flugwissenschaften*, Vol. 11, 1963, p. 265.

[5] Laschka, B., "Das Potential und das Geschwindigkeitsfeld der harmonisch schwingenden tragenden Fläche bei Unterschallströmung," *Zeitschrift für angewandte Mathematik und Mechanik*, Vol. 43, 1963, pp. 325–333; also "Erratum," *Zeitschrift für angewandte Mathematik und Mechanik*, 1967, p. 284.

[6] Laschka, B. and Schmid, H., "Interference between wing and horizontal/vertical tail in unsteady subsonic flow," Rept. M-51/68, 1968, Vereinigte Flugtechnische Werke, Munich.

[7] Watkins, C. E., Runyan, H. L., and Woolston, D. S., "On the kernel function of the integral equation relating the lift and downwash distributions of oscillating finite wings in subsonic flow," Rept. 1234, 1955, NACA.

[8] Laschka, B., Müller, A., and Böhm, G., "Calculation of the pressure distribution of integral lifting surfaces in subsonic flow including the deformation of the wake," Rept. M-71/66, 1966, Vereinigte Flugtechnische Werke, Munich.

[9] Topp, L. J., Rowe, W. S., and Shattuck, A. W., "Aeroelastic consideration in the design of variable sweep aeroplanes," ICAS-Paper 66-12, 1966, 5th ICAS Congress, London.

[10] Laschka, B. and Schmid, H., "Unsteady aerodynamic forces on coplaner lifting surfaces in subsonic flow (wing-horizontal tail interference)," AGARD Structures and Materials Panel Meeting, Ottawa, Canada, Sept. 25–27, 1967; also *Jahrbuch 1967 der Wissenschaftliche Gesellschaft für Luft- und Raum-fahrt*, pp. 211–222.

[11] Wittmeyer, H., "Aeroelastomechanische Untersuchungen an dem Flugzeug SAAB 37, Viggen," Ludwig Prandtl Memorial Lecture, 6th ICAS Congress, Munich, Sept. 1968.